Volume 12
Number 24
21 December 2024
Pages 6155-6418

Biomaterials Science

rsc.li/biomaterials-science

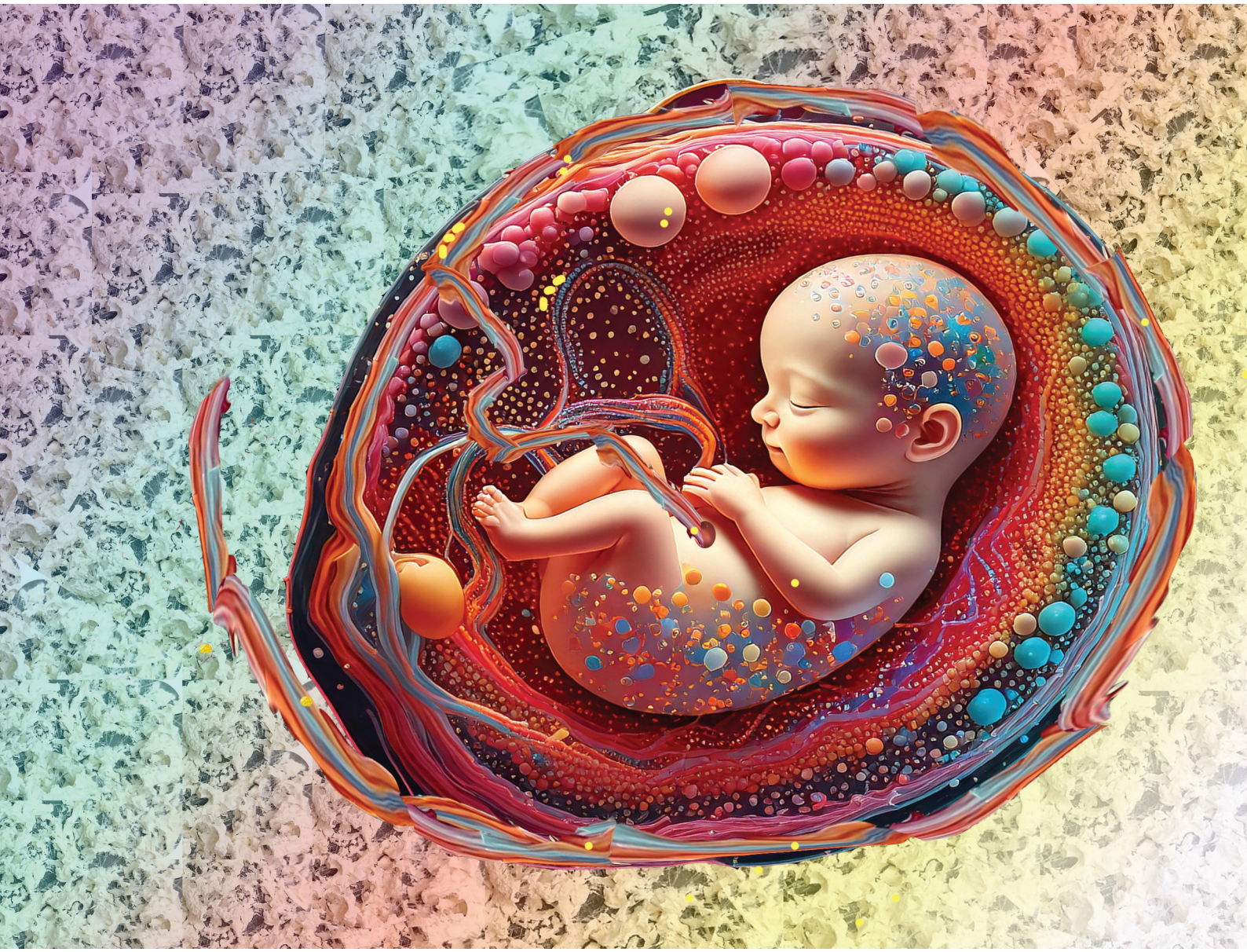

ISSN 2047-4849

ROYAL SOCIETY OF CHEMISTRY

PAPER
Cheng-Fong Chen *et al.*
Wharton's jelly of the umbilical cord serves as a natural biomaterial to promote osteogenesis

European Society for Biomaterials

Biomaterials Science

ROYAL SOCIETY OF CHEMISTRY

PAPER

View Article Online
View Journal | View Issue

Cite this: *Biomater. Sci.*, 2024, **12**, 6284

Wharton's jelly of the umbilical cord serves as a natural biomaterial to promote osteogenesis†

Yu-Show Fu, ‡[a] Shang-Wen Tsai,[b,c] Zhen-Jie Tong,‡[d] Chang-Ching Yeh,[e,f,g] Tien-Hua Chen[h,i,j,k] and Cheng-Fong Chen *[b,c]

Various factors can contribute to bone damage or loss, presenting challenges for bone regeneration. Our study explores the potential clinical applications of two processed forms of Wharton's jelly of the human umbilical cord for treating bone loss. Wharton's jelly from fresh umbilical cords underwent two distinct processes: (1) frozen Wharton's jelly (WJF), preserved with cryoprotective agents, and (2) decellularized Wharton's jelly matrix (WJD), prepared only *via* lyophilization without cryoprotectants. Both WJD and WJF are rich in collagen, hyaluronan, and polysaccharide proteins. Notably, WJD exhibited a porous structure lacking nuclei from human umbilical cord mesenchymal stem cells, unlike WJF. In direct contact experiments, WJD stimulated osteoblast migration, enhanced osteoblast maturation, and promoted calcium deposition for bone formation when administered to cultured rat osteoblasts. Furthermore, in transwell co-culture experiments, both WJD and WJF increased the rat osteoblast expression of RUNX2 and OPN genes, elevated alkaline phosphatase levels, and enhanced extracellular calcium precipitation, indicating their role in osteoblast maturation and new bone formation. Hyaluronic acid, one of the ingredients from WJD and WJF, was identified as a key component triggering osteogenesis. *In vivo* experiments involved creating circular bone defects in the calvarias of rats, where WJD and WJF were separately implanted and monitored over five months using micro-computerized tomography. Our results demonstrated that both WJD and WJF enhanced angiogenesis, collagen formation, osteoblast maturation, and bone growth within the bone defects. In summary, WJD and WJF, natural biomaterials with biocompatibility and nontoxicity, act not only as effective scaffolds but also promote osteoblast adhesion and differentiation, and accelerate osteogenesis.

Received 31st December 2023,
Accepted 18th September 2024

DOI: 10.1039/d3bm02137h

rsc.li/biomaterials-science

[a]*Department of Anatomy and Cell Biology, National Yang Ming Chiao Tung University, Taipei, Taiwan, Republic of China*
[b]*Division of Joint Reconstruction, Department of Orthopaedics and Traumatology, Taipei Veterans General Hospital, Taipei, Taiwan, Republic of China. E-mail: cf_chen@vghtpe.gov.tw; Fax: +886-2-28757657; Tel: +886-2-28757557*
[c]*Department of Orthopaedics, School of Medicine, National Yang Ming Chiao Tung University, Taipei, Taiwan, Republic of China*
[d]*Institute of Anatomy and Cell Biology, National Yang Ming Chiao Tung University, Taipei, Taiwan, Republic of China*
[e]*Department of Obstetrics and Gynecology, Taipei Veterans General Hospital, Taipei, Taiwan, Republic of China*
[f]*Department of Obstetrics and Gynecology, National Yang Ming Chiao Tung University, Taipei, Taiwan, Republic of China*
[g]*Department of Nurse-Midwifery and Women Health, National Taipei University of Nursing and Health Sciences, Taipei, Taiwan*
[h]*Department of Post-Baccalaureate Medicine, College of Medicine, National Chung Hsing University, Taichung City, Taiwan*
[i]*Institute of Anatomy and Cell Biology, School of Medicine, National Yang Ming Chiao Tung University, Taipei, Taiwan, Republic of China*
[j]*Trauma Center, Department of Surgery, Taipei Veterans General Hospital, Taipei, Taiwan, Republic of China*
[k]*Division of General Surgery, Department of Surgery, Taipei Veterans General Hospital, Taipei, Taiwan, Republic of China*

†Electronic supplementary information (ESI) available. See DOI: https://doi.org/10.1039/d3bm02137h

‡These two authors have made equal contributions to this manuscript.

1. Introduction

Bones may be damaged or lost due to trauma, fracture, bacterial infection, or tumor metastasis and invasion. When the bone loss is greater than two times the diameter of the diaphysis, known as the critical-sized bone defect, the defect cannot naturally heal despite implanting various bone regenerative materials.[1] Furthermore, the risks of reduced weight-bearing capability and subsequent fractures are increased.

Currently, common clinical bone materials are generally divided into three types. The first type is autologous bone graft whereby bone tissues from other body parts are surgically obtained and used to fill up the bone defect region. The drawbacks of this method include a long recovery period, the requirement of two invasive surgeries, and the amount/area of bone graft may not be large enough. The second type is allogeneic bone graft, *i.e.*, excessive bone tissue removed from other patients who required surgical treatment. In addition to ethical issues, the risks of disease transmission are present. The third type is artificial bone materials, which require research and development of new synthetic bone materials for

clinical applications. Bone engineering depends on the design of scaffolds, which are highly porous three-dimensional constructs that can hasten the regeneration of damaged tissues and organs by offering an ideal environment for cell growth and differentiation.[2] Hence, a hydrogel, a 3D network of a hydrophilic polymer material which can quickly absorb and retain water, has been widely used in tissue engineering.[3] Hydrogels can be categorized as natural, synthetic, and semi-natural based on their source material. Natural hydrogels are biocompatible and biodegradable, but have low mechanical endurance. Synthetic hydrogels have lesser biocompatibility but greater mechanical strength to bear weight. Semi-synthetic hydrogels can be composed of both natural and synthetic polymers.[4] There are still obstacles to be resolved in the field of bone engineering. In this work, we propose a new approach based on Wharton's jelly from the umbilical cord for bone regeneration.

The umbilical cord contains two arteries and one vein. The connective tissue wrapping around these blood vessels, called Wharton's jelly, is a three-dimensional structure composed of a considerable amount of extracellular matrix. Wharton's jelly can serve as a scaffold for various cell types to increase cell adhesion of adipose mesenchymal stem cells, hematopoietic stem cells, chondrocytes, vascular endothelial cells, and fibroblasts and thereby promote skin healing, cartilage repair, and blood vessel reconstruction.[5–9]

In addition to serving as a scaffold for cells and a scaffold for tissue engineering, Wharton's jelly contains a substantial amount of extracellular matrix components such as collagen, hyaluronic acid, fibronectin, and sulfated proteoglycan.[8,10,11] Collagen fibrils are the main non-mineral component of bone tissue.[12] Collagen or collagen-based biomaterials are mostly used for the treatment of bone tissue regeneration.[13,14] Another main component, hyaluronic acid, is found throughout the human body and is widely distributed in the connective tissue of the dermis, synovial fluid, the dental pulp matrix, and other parts of the body.[15] Hyaluronic acid or hyaluronic acid-based scaffolds can promote wound healing, cartilage repair and bone regeneration when they are added to artificial or synthetic materials.[15–24] In the present study, we aimed to investigate the effect of Wharton's jelly on osteoblasts and bone regeneration.

We prepared two types of Wharton's jelly. For the first type, Wharton's jelly was cryopreserved using cryoprotective agents and was named Frozen Wharton's jelly (WJF). WJF was applied immediately after thawing, when it still contained human umbilical cord mesenchymal stem cells (HUMSCs). For the second type, Wharton's jelly was lyophilized and dissolved in normal saline. Since it no longer contained umbilical cord mesenchymal stem cells, the final product was named Decellularized Wharton's jelly matrix (WJD). Our results indicated that both WJF and WJD could not only promote cell adhesion, differentiation, and maturation of rat osteoblasts *in vitro*, but also help in bone regeneration in rats with critical-sized calvarial defects.

2. Materials and methods

2.1. Preparation of Wharton's jelly

Human umbilical cords were aseptically collected after delivery and kept in cold (4 °C) Hank's Balanced Salt Solution (HBSS; Gibco 14185-052). Wharton's jelly was isolated within 24 h after collection. All experimental instruments were autoclaved, disinfected in 75% ethanol, and flamed before use. In a laminar hood, umbilical cords were disinfected by soaking in 75% ethanol, placed in HBSS, and incised longitudinally. The umbilical vessels were readily visible and could be removed using forceps. After the detachment and withdrawal of the blood vessels, we obtained Wharton's jelly, which appeared as milky white interstitial tissues. They were then cut, using a trephine drill, into 8 mm diameter discs, with a thickness of 2 mm each.

2.2. Processing of Wharton's jelly to obtain WJF and WJD

The isolated Wharton's jelly was subsequently processed using the following two methods: 1. Frozen Wharton's Jelly (WJF): freshly obtained Wharton's jelly was immediately frozen in the presence of cryoprotective agents (10% DMSO in 10% FBS DMEM). WJF was readily used after thawing when it still contained HUMSCs. 2. Decellularized Wharton's jelly matrix (WJD): freshly obtained Wharton's jelly was stored in a −80 °C refrigerator for 24 hours, followed by lyophilization for 3 hours (0.15 to 0.2 torr at −50 °C) using a freeze dryer, which resulted in WJD without HUMSCs. WJF and WJD in disc shape were individually paraffin-embedded and subjected to histochemical staining to examine their histological structures. These disc-shape WJF and WJD were used in the *in vitro* and *in vivo* experiments described in later sections.

2.3. Sirius red staining

Sirius red was applied to label the collagen in the tissues. WJF and WJD were paraffin-embedded. The tissue sections were stained using 0.1% Sirius red (Sigma 2610-10-8) in picric acid for 14 minutes. Subsequently, the tissue sections were washed by immersing in ddH_2O. The tissue sections were then dehydrated by immersing in a series of increasing concentrations of alcohol, followed by immersing in xylene. Finally, the section slides were mounted with the mounting medium and examined *via* an optical microscope.

2.4. Periodic acid-Schiff (PAS) staining

PAS stain was applied to label (in pink) the polysaccharides (hyaluronic acid), glycogen and glycoproteins in the tissues. WJF and WJD were paraffin-embedded. The tissue sections were stained, *via* a PAS Stain Kit (Sigma 395B-1KT), in periodic acid solution for 5 minutes, washed in ddH_2O, in Schiff's reagent for 15 minutes, and then washed in ddH_2O. Following dehydration with alcohol and immersion in xylene, the sections were mounted with the mounting medium and then examined *via* an optical microscope.

2.5. Alcian blue staining

An Alcian blue stain kit (Abcam ab150662) was used to label mucins in the tissues. WJF and WJD were paraffin-embedded.

The tissue sections were first stained with acetic acid for 3 minutes and then by Alcian blue solution (pH = 2.5) for 15 minutes at 37 °C. Following dehydration with alcohol and immersion in xylene, the sections were mounted with the mounting medium and then examined *via* an optical microscope.

2.6. Immunohistochemical staining for WJF and WJD

In order to identify the distribution of the extracellular matrix in WJF and WJD, WJF and WJD sections were reacted with primary antibodies of rabbit anti-collagen I antibody (Abcam, ab34710, 1 : 200), rabbit anti-collagen III antibody (Abcam, ab23746, 1 : 200), and rabbit anti-fibronectin antibody (Abcam, ab23751, 1 : 200) at 4 °C for 18 hours to recognize the collagen I, collagen III, and fibronectin respectively. Subsequently, secondary antibody goat anti-rabbit-IgG-conjugated biotin (Abcam, ab6720, 1 : 250) was added to react for 1 hour at room temperature, followed by the addition of avidin-biotinylated-horseradish peroxidase complex (ABC Kit, Vector Laboratories) (Vector Laboratories PK-4000, VECTASTAIN®) for 1 hour at room temperature. Finally, DAB (5 mg DAB, 35% H_2O_2 3.5 μL in 10 mL Tris-HCl, pH 7.4) was added for color development.

2.7. WJD processing for scanning electron microscopy (SEM) and energy dispersive X-ray spectroscopy (EDS)

Lyophilized WJD containing no mesenchymal stem cells were immersed in a fixative solution containing 2% paraformaldehyde and 2% glutaraldehyde, placed in a 4 °C refrigerator for 24 hours, and followed by fixation with 2% osmium tetroxide (OsO_4) solution. At this point, WJD was oxidized into a black tissue block, which was washed with 0.1 M phosphate-buffered saline (PBS) to remove the residual fixative solution and then dehydrated with alcohol. Subsequently, the specimens were dried by critical point drying with liquid carbon dioxide (35 °C at 1072 psi) to remove the ethanol inside the specimens. Critical point drying was typically employed to prevent shrinkage and deformation during the drying process. The specimens, after being subjected to gold coating to protect their ultra-structure on the surface from electron beam-induced thermal damage, were ready for SEM scanning (JSM-7600F, JEOL) and EDS analysis (X-MaxN, OXFORD instruments).

2.8. *In vitro* culture of rat osteoblasts (ROBs)

One-day-old Sprague Dawley (SD) rats were sacrificed *via* anesthetic overdose. In a laminar flow cabinet, the calvarias of the rats were obtained using sterilized instruments and cut into cubes with a side length of 1 mm, followed by washing with sterile HBSS to remove red blood cells. The tissues were then reacted with 0.1% trypsin and 0.1% collagenase for 2 hours at 37 °C under shaking. Subsequently, Dulbecco's Modified Eagle's medium (DMEM) with 10% fetal bovine serum (FBS) was added to neutralize the effect of trypsin, followed by centrifugation at 1500 rpm for 5 minutes. The cells attached at the bottom were re-suspended in DMEM with 10% FBS. The cells were seeded in a 10 cm culture dish, and the culture medium was changed every 4 days. After 10 to 14 days, a full confluence could be reached, and the cells were then passaged. Osteoblasts in the second passage were used in this study.

2.9. Rat osteoblasts and WJD in the direct contact coculture system

2×10^4 rat osteoblasts were cultured in a 24-well plate and kept in 10% FBS DMEM for one day before WJD was added. WJD were post-fixed, paraffin-embedded, and sectioned for staining at 1, 7, 14, and 21 days after being co-cultured with osteoblasts in direct contact. HE staining was utilized to observe the morphology of WJ and rat osteoblasts, whereas Alizarin red S staining was employed to observe the calcification in WJD. After 21 days of co-culture, the osteoblasts and mineral granules in the WJD were examined using SEM scanning and EDS analysis.

2.10. Grouping of rat osteoblasts and WJD/WJF using the transwell coculture system

Rat osteoblasts cultured *in vitro* were divided into five groups as follows:

1. The ROB group: 2×10^4 rat osteoblasts per well were cultured alone in a 24-well plate.

2. The ROB/WJD group: 2×10^4 rat osteoblasts per well were seeded in the lower chamber of 24-well plate, and WJD was added to the top chamber of the transwell. There was no direct contact between the osteoblasts and WJD.

3. The ROB/WJF group: 2×10^4 rat osteoblasts per well were seeded in a lower chamber of the 24-well plate, and WJF was added to the top chamber of the transwell. There was no direct contact between the osteoblasts and WJF.

4. The ROB + LHA group: 2×10^4 rat osteoblasts per well were cultured in DMEM supplemented with low molecular weight hyaluronic acid (LHA, 60 kDa, 1 mg mL^{-1}) for 21 days.

5. The ROB + HHA group: 2×10^4 rat osteoblasts per well were cultured in DMEM supplemented with high molecular weight hyaluronic acid (HHA, 1500 kDa, 1 mg mL^{-1}) for 21 days.

6. The ROB + COL1 group: 2×10^4 rat osteoblasts per well were cultured in DMEM supplemented with type 1 collagen (COL1, 125 μg mL^{-1}, Sigma C8919) for 7 days.

The culture medium (DMEM with 10% FBS) was changed every 3 days. Bone-related features were assessed after 7-, 14-, or 21-days of culturing.

2.11. RT-PCR and real-time RT-PCR

Rat osteoblasts cocultured for 7 days were treated with 0.05% trypsin to be harvested. The cells were then reacted with TRIzol (Sigma T9424) to extract total RNA. The purified RNA (3 μg) was transcribed to complementary DNA (cDNA) *via* reverse transcription, followed by the manufacturer's instructions of RevertAid Reverse Transcriptase (Thermo Fisher Scientific). The cDNA was subjected to polymerase chain reaction (PCR) with primers and a master mix. The following primers were applied:

Rat-runt-related transcription factor 2 (Rat-*RUNX2*) (212 bp)
Forward: 5′-GCTTCTCCAACCCACGAATG-3′
Reverse: 5′-GAACTGATAGGACGCTGACGA-3′
Rat-alkaline phosphatase (Rat-*ALP*) (71 bp)

Forward: 5′-ACGAGGTCACGTCCATCCT-3′
Reverse: 5′-CCGAGTGGTGGTCACGAT-3′
Rat-osteopontin (Rat-*OPN*) (121 bp)
Forward: 5′-CCCGATGCCACAGATGAG-3′
Reverse: 5′-TCCCGTTGCTGTCCTGAT-3′
Rat-GAPDH (160 bp)
Forward: 5′-CTCTACCCACGGCAAGTTCAAC-3′
Reverse: 5′-GGTGAAGACGCCAGTAGACTCCA-3′

The PCR final products were analyzed using 2% agarose gel electrophoresis and photographed with a UV transilluminator. In addition, the real-time qPCR analysis of cDNA mixed with primers and SYBR Green Master Mix (Vazyme Q711) was detected by StepOnePlus™ Real-Time PCR System (Applied Biosystems). GAPDH was used as an internal control for RT-qPCR, and the results were presented by comparing it to the control groups.

2.12. Cell alkaline phosphatase (ALP) staining

Rat osteoblasts cocultured for 14 days were treated with 5-bromo-4-chloro-3-indolyl phosphate/nitro blue tetrazolium solution (Sigma B5655) for 1 hour in a 37 °C oven in the dark. Subsequently, SDS in 10% HCl was added and reacted for 12 hours in a 37 °C oven while keeping in the dark. Finally, the absorbance of the supernatant at 595 nm, which represents the expression level of ALP, was measured.[25] A higher expression of ALP indicates a larger number of matured osteoblasts.

2.13. Alizarin red S staining

Rat osteoblasts of ROB, ROB/WJD, and ROB/WJF groups were cultured for 21 days (the medium was changed every 3 days). The cells were fixed using 2.5% glutaraldehyde for 15 minutes and then stained with 2% alizarin red S (Sigma A5533, pH = 4.1–4.3) for 1 hour in a 37 °C oven in the dark. Subsequently, 10% cetylpyridinium chloride (Sigma C-0732) was added to react for 1 hour in a 37 °C oven in the dark. The absorbance of the supernatant at 540 nm was measured. A higher absorbance indicates a higher level of calcium precipitation.[26]

2.14. Development of the rat calvarial critical-sized bone defect model

Eight-week-old male SD rats, weighing 250 to 280 g, were anesthetized *via* intraperitoneal injection of Zoletil 50 and xylazine hydrochloride (Sigma 23076359). The rat's head was fixed in a stereotaxic apparatus and the hair was shaved with a razor. The rat's skin was then disinfected with iodine solution-dipped cotton ball and incised with a scalpel. The subcutaneous tissues were pushed away using a surgical scissor, and the periosteum was removed. Subsequently, a surgical trephine bur (8 mm in diameter) was applied to drill the calvaria, and the calvaria was detached from the underlying dura to serve as a critical-sized bone defect animal model. Finally, the subcutaneous tissues and skin were sutured.

2.15. Grouping of experimental animals

SD rats were grouped into three study groups:

1. Injury + Saline group: no treatment but saline was given following calvarial bone defect (Fig. 4A).

2. Injury + WJD group: dissolved WJD in saline (disc-shaped WJD with a diameter of 8 mm and a thickness of 2 mm) was administered to the defect region immediately after calvarial bone defect (Fig. 4A).

3. Injury + WJF group: dissolved WJF (disc-shape WJF with a diameter of 8 mm and a thickness of 2 mm) was administered to the defect region immediately after calvarial bone defect (Fig. 4A).

Immunosuppressants were not administered to the rats in the two transplantation groups mentioned above. Our previous studies have shown that the transplantation of umbilical cord mesenchymal stem cells does not trigger immunological responses; hence, immunosuppression may be unnecessary.[27–32]

2.16. Micro-computerized tomography scan (micro-CT)

Micro-CT images were processed with AMIDE software (SOURCEFORGE) to reconstruct 3-dimensional radiographic images. A small animal computed tomography system (U-CTUHR, MI Labs) was applied in the present study to scan the calvarias of live rats on day 1 after surgery and monthly at months 1, 2, 3, 4, and 5 to follow-up the healing levels of the calvarial bone defect.

2.17. Sacrifice, perfusion fixation, decalcification, and paraffin sections of experimental animals

SD rats were sacrificed *via* anesthetic overdose and fixed *via* the perfusion of 4% paraformaldehyde and 7.5% picric acid in 0.01 M PBS. The calvarias were obtained and placed in a fixative solution for 24 hours. For decalcification, calvarias were then immersed in 20% EDTA in 9% NaOH solution for 9 days, with the solution changed every 3 days. The decalcified calvarias were washed in running water for 8 hours, followed by dehydration with ethanol solution and xylene, and paraffin-embedded with pure paraffin. Subsequently, the samples were horizontally sectioned into 7 μm thick tissue slices with a microtome and subjected to various staining (ESI Fig. 1†).

2.18. Hematoxylin & eosin (H&E) stain

Tissue sections (7 μm thick) were deparaffinized, rehydrated, stained with hematoxylin (Muto Pure Chemicals; no. 3008-1) for 5 minutes, and stained with eosin (Muto Pure Chemicals; no. 3008-2) for 1 minute. The sections were then washed with water, dehydrated with ethanol, and treated with xylene. Finally, the slides were mounted with the mounting medium for examination and photography using an optical microscope. The slice with the largest area of cranial tissue was obtained, and the circumference of the boundaries between the old and newly formed bone was marked with dashed lines for quantification of the original area of bone defect. Subsequently, the newly formed bone within the bone defect region was quantified and expressed in percentage.

2.19. Goldner's trichrome staining

Calvarial tissue sections with a thickness of 7 μm were deparaffinized, rehydrated, and stained with the mixture of hematoxylin A and hematoxylin B for 10 minutes. The sections were

then stained with the ponceau fluid for 1 minute, followed by immersing in 0.1% acetic acid for 10 seconds. Subsequently, the sections were stained with orange G for 40 minutes and immersed in 0.1% acetic acid for 5 minutes. Finally, the sections were stained with light green G solution for 30 minutes and immersed in 0.1% acetic acid for 5 minutes. The final stained sections showed that the nuclei were stained in dark brown, muscles in red, and collagen within the bone in green. The slice with the largest area of the calvarial tissue was obtained, and the circumference of the boundaries between the old and newly formed bone was marked with dashed lines for quantification of the original area of bone defect. Subsequently, the green collagen within the bone defect region was quantified and expressed in percentage.

2.20. Alkaline phosphatase (ALP) staining

Calvarial tissue sections with a thickness of 7 μm were deparaffinized, rehydrated, and reacted with an alkaline phosphatase kit (Sigma 85L2-1KT) for 1 hour in a 37 °C oven, followed by immersion in ddH_2O. A cell stained in purple indicated that its cytoplasm contained ALP, *i.e.*, the cell was a mature osteoblast.

The slice with the largest area of calvarial tissue was obtained, and the circumference of the boundaries between the old and newly formed bone was marked with dashed lines for quantification of the original area of the bone defect. Subsequently, the purple area where mature osteoblasts occupied within the bone defect region was quantified and expressed in percentage.

2.21. Anti-osteocalcin antibody immunohistochemical staining

Following deparaffinization and rehydration of 7 μm cranial tissue sections, the primary mouse anti-osteocalcin antibody (Abcam ab13740, 1 : 200) was added to react for 16 to 18 hours at 4 °C. Subsequently, secondary goat anti-mouse-IgG-conjugated biotin (Millipore AP124B, 1 : 250) was added to react for 1 hour at room temperature, followed by the addition of the avidin-biotinylated-horseradish peroxidase complex (ABC Kit, Vector Laboratories) (Vector Laboratories PK-4000, VECTASTAIN®) for 1 hour at room temperature. The sections were then washed thrice with 0.01 M PBS for 5 minutes. Finally, DAB (5 mg DAB, 35% H_2O_2 3.5 μL in 10 mL Tris-HCl, pH 7.4) was added for color development. The dark brown area within the bone defect region (*i.e.*, the area of osteocalcin) was quantified to represent the activity of bone formation.

2.22. Histochemical staining of *Griffonia simplicifolia* lectin I (GSL I-B4)

Griffonia simplicifolia 1 – lectin (GSL1-B4) (Vector Laboratories) was a marker of capillaries and microcirculatory vessels.[33] GS1-lectin was stored in a 4 °C refrigerator. In this study, 2 mg mL^{-1} GS1-lection was diluted to 25 μg mL^{-1} GS1-lectin with 0.1 M PBS. Cranial sections with a thickness of 7 μm were stained with 25 μg mL^{-1} fluorescent lectin for 60 minutes while protecting from light and then washed thrice with 0.1 M PB, 5 minutes each. Sections were then mounted with the mounting medium and examined and photographed with fluorescence microscopy to analyze the distribution of blood vessels.

2.23. Statistical analysis

All experimental data were expressed in mean ± standard deviation. One-way ANOVA was applied for comparing the mean of each study group, and two-way ANOVA was applied, followed by Fisher's least significant difference (LSD) test for multiple comparisons. A value of $p < 0.05$ was considered the lowest standard for statistical significance.

3. Results and discussion

3.1. Morphological features and compositions of WJD and WJF tissues

With H&E staining, lyophilization of WJD showed a porous morphology with an extracellular matrix forming a web-like structure surrounding the pores. Besides, no HUMSCs were observed in WJD. In WJF, nuclei of HUMSCs could be observed, with extracellular matrix aligned in compact, organized bundles (Fig. 1A). We further labeled collagen, hyaluronic acid, and muscins in the tissues, with Sirius red, PAS, or the Alcian blue reagent, respectively. The results showed that in WJD, collagen, hyaluronic acid, and muscins formed a bundle structure surrounding the pores; whereas in WJF they formed a regular bundle structure (Fig. 1A). WJD appears as a white dry tissue, whereas WJF appears as a translucent and gelatinous tissue mass after dissolving in normal saline. In order to mark the distribution of collagen I, collagen III, and fibronectin, anti-collagen I, collagen III, and fibronectin antibodies were used. Collagen I, collagen III, and fibronectin formed a net-like structure surrounding the pores in WJD, whereas they developed normal bundle structures in WJF (Fig. 1B). The SEM magnified image of WJD reveals that the bundle structure surrounding the pores is composed of regular and dense cable-like constructions bunched together (Fig. 1C). The abundance and organization of extracellular matrices in WJ indicates that the WJD/WJF is more suited to intergrade with trabecular or porous bone. The stroma of Wharton's jelly contained high levels of type I, III, IV, and V collagens, hyaluronic acid, and several sulfated glycosaminoglycans.[8,10,11] Collagen, the most abundant protein in mammals, is known to be the main constituent of the extracellular matrix. Collagen is a relatively simple protein that provides structure, protection, and support for human tissues. Its chains are primarily made of three basic amino acids, glycine, proline, and hydroxyproline.[34] Because of its natural abundance, biocompatibility and biodegradability, high permeability, and minimal immunogenic reaction, collagen or collagen – based scaffolds have been widely studied in wound healing and bone tissue engineering.[13,35,36] Numerous studies have shown that hyaluronic acid or hyaluronic acid – based biomaterials/scaffolds are used as tissue engineering tools to enhance the efficacy of regenerative medicines.[15–24]

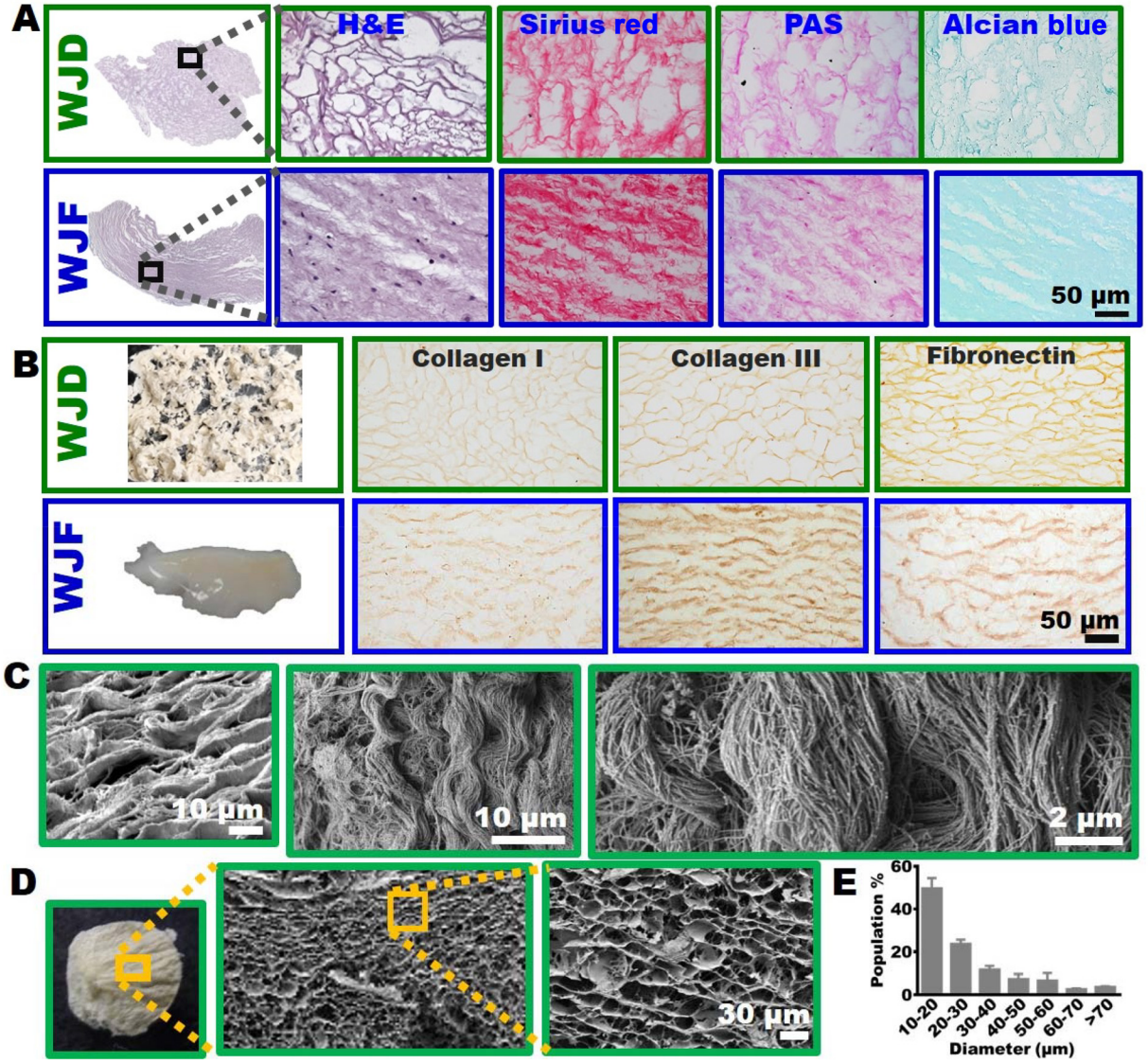

Fig. 1 Histological and morphological analysis of WJD and WJF. WJD and WJF were paraffin-embedded, sectioned, and subjected to H&E, Sirius red, PAS, and Alcian blue staining. WJD had a porous structure whereas WJF had a compact structure and contained HUMSCs. Both WJD and WJF contained a large amount of collagen, glycoproteins, hyaluronic acid and mucins (A). The distribution patterns of collagen I, collagen III, and fibronectin in WJD and WJF (B). SEM high-magnification pictures reveal regular, dense, and bundled filament structures encircling the pores of WJD (C). WJD showed a porous structure with various pore sizes under SEM (D), with pore diameters in the range of 10 to 70 microns (E).

Freeze-dried WJD resembles the bone structure in appearance. SEM images, from low to high magnification, revealed densely distributed pores with different diameters, in the range of 10 to 70 microns in WJD (Fig. 1D and E). Porosity is an important criterion for a scaffold to promote new bone formation. The effects of pore sizes on new bone formation have been studied. Based on the results from the published papers, scaffolds suitable for osteoblast adhesion, differentiation, and maturation varied with their pore size and compositions.[37–39] To date, with the advancement of nanofabrication technology, the pore size could be far below 5 μm and made even smaller.[40] The size of osteoblasts, assessed with SEM, was around 5 to 10 μm.[38] Why could these materials promote bone regeneration? We agree with the proposal that the growth and differentiation of osteoblasts were triggered as long as the pore size was large enough to allow osteoblasts to achieve local adhesions or to render their processes to get into the pore.[40] In the present study, the pore sizes of WJD were generally less than 70 μm, with around 80% of pore diameters in the range of 10 to 30 μm. Hence, we believed that the pore sizes were sufficient for osteoblast adhesion and maturation.

3.2. WJD promoted adhesion and maturation of osteoblasts in the direct contact coculture system

Rat osteoblasts were cultured in a 24-well plate and maintained in 10% FBS DMEM for one day before adding WJD. The pores of WJD gradually disappeared or diminished in one day by absorption of DMEM, demonstrating the great water

absorption capacity of WJD. After one week, rat osteoblasts appeared in WJD. After two weeks, not only that the nuclei size of rat osteoblasts in WJD increased, the osteoblasts also formed processes. After three weeks, rat osteoblasts in WJD were found in lacunae-like structures. It indicated that WJD was a good scaffold to attract adhesion of osteoblasts and promote maturation of osteoblasts (Fig. 2A). Furthermore, alizarin red S staining to label calcium revealed that numerous calcium deposits occurred in WJD after two weeks after WJD placement. Calcium accumulation increased in three weeks (Fig. 2B). After three weeks, the SEM images demonstrated that an abundance of osteocyte processes in the WJD, as well as mineral-like substance around the processes (Fig. 2C–E). Next, we analyzed the elemental composition using EDS. The results show that the mineralized substance is rich in calcium, about 69.3 ± 1.2% (Fig. 2D and D1). The filament-like structures contain a lot of carbon and oxygen molecules but very little calcium. They appear to be organic components, suggesting that they might be cell processes of osteocyte (Fig. 2E and E1). Our results show that WJD can attract osteoblast migration, differentiation, and maturation, and consequently can promote calcium accumulation and stimulate bone formation. A number of studies have demonstrated that decellularized Wharton's jelly matrix could serve as a great scaffold for

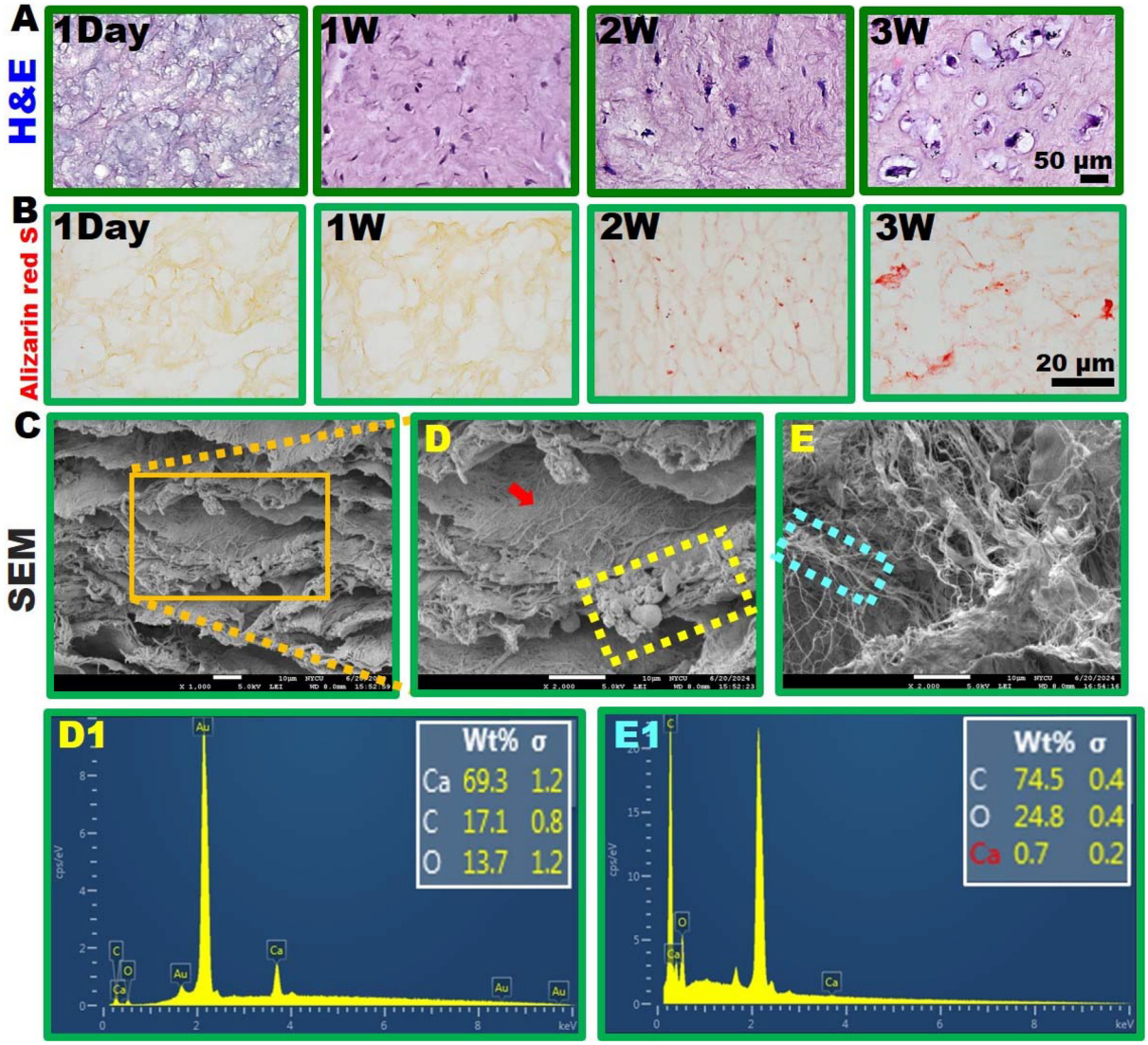

Fig. 2 WJD promoted the migration and maturation of osteoblasts and accelerated bone formation in the direct contact coculture system. Rat osteoblasts were cultured in a 24-well plate and WJD was added after one day. (A) Rat osteoblasts migrated into the WJD in one week, whereas many cell processes appeared in two weeks, and bone lacuna-like structures were formed in three weeks. (B) The alizarin red S staining results demonstrated that abundant calcium deposits occurred in WJD in Week 2 and Week 3 (red). SEM images of WJD co-cultured with rat osteoblasts for 3 weeks at low magnification (C) and high magnification (D and E) reveal many osteocyte processes in WJD (arrows). The composition analysis of the crystal structure in the D (yellow dashed rectangle) and the cell process in E (blue dashed rectangle) by EDS show high calcium (D1) and carbon molecules (E1), respectively. The specimen is gold-coated, thus the gold composition is extremely high.

various types of cells except osteoblasts.[5–9] For example, it has been demonstrated that decellularized Wharton's jelly, used as a scaffold and planted with adipose mesenchymal stem cells *in vitro* for 4 weeks, could trigger the adipose mesenchymal stem cells to differentiation into chondrocyte for joint repair.[6] Besides, a 3-dimensional vessel structure formed with decellularized Wharton's jelly and silk (silk tissue-engineered vascular grafts) could promote proliferation and activation of vascular endothelial cells to form a blood vessel structure capable of vasoconstriction.[7] Decellularized Wharton's jelly matrix could also promote wound healing of skin[8,9] and improved hematopoietic stem cells' proliferation, activity, and ability of differentiation.[5]

3.3. WJD/WJF promoted osteogenic differentiation of rat osteoblasts under co-cultivation without direct contact

We cultured rat osteoblasts in the lower chamber of a transwell coculture system, WJD or WJF into the top chamber to avoid direct contact between WJD/WJF and osteoblasts. After 7 days of coculturing with DMEM supplemented with 10% FBS, osteoblasts in the lower chamber from each study group were harvested for rat *RUNX2* RT-PCR. Rat *RUNX2* expression was detected in the osteoblasts of the ROB, ROB/WJD, and ROB/WJF groups (Fig. 3A). Furthermore, rat *RUNX2* was quantified using real-time RT-PCR, which showed that the expression level of rat *RUNX2* was significantly increased in the ROB/WJD and ROB/WJF groups when compared to the ROB group (Fig. 3B). Bone development and maturation progresses through various stages, including bone marrow mesenchymal cells, osteo-progenitors, pre-osteoblasts, osteoblasts, and osteocytes. Various genes have risen and fallen at different stages. RUNX2 is an early stimulator of bone differentiation.[41]

We further examined the ALP expression level in rat osteoblasts after 14-day of coculture with WJD or WJF. The results indicated that the ALP expression level significantly increased in the ROB/WJD and the ROB/WJF groups compared to that of the ROB alone group (Fig. 3C and D). Subsequently, the rat osteoblasts in the lower chamber of transwell were stained

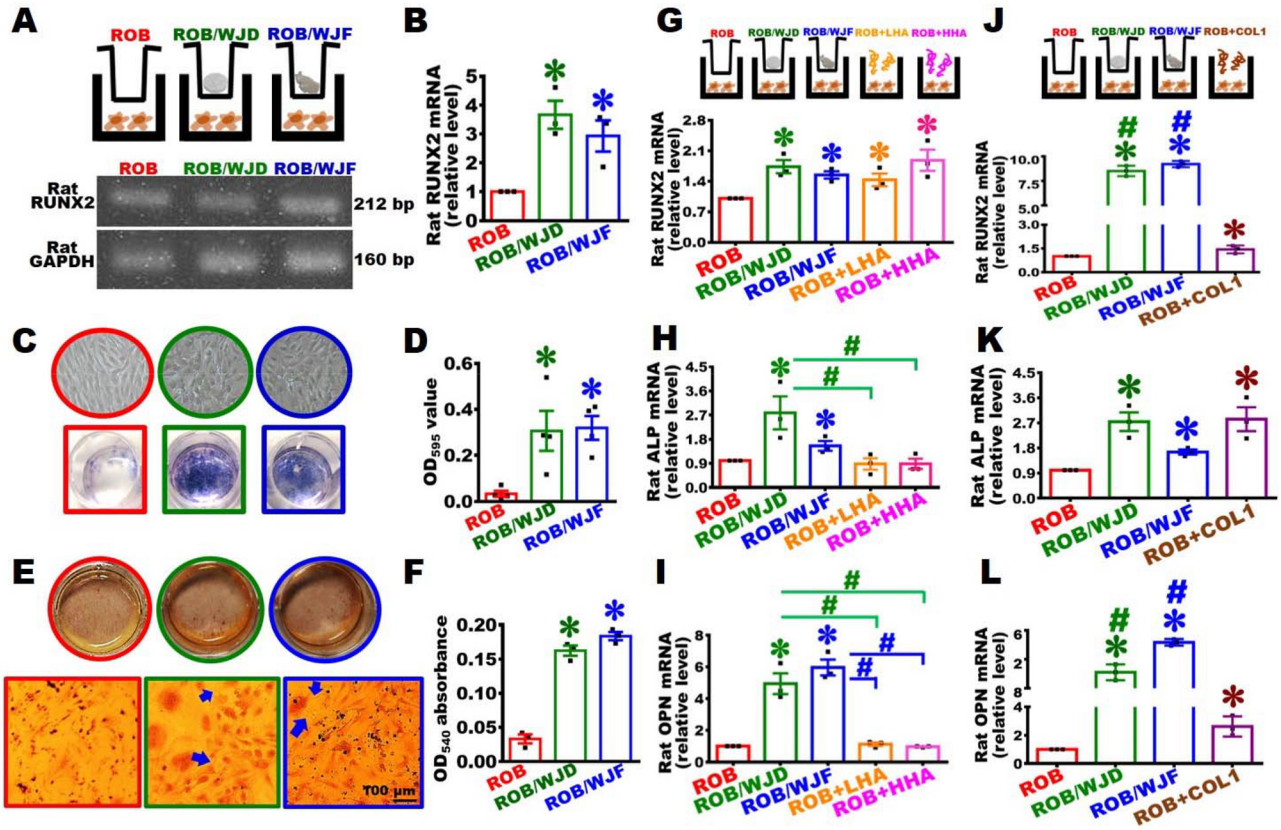

Fig. 3 Components of WJD/WJF promoted osteogenic differentiation of rat osteoblasts. WJD/WJF was added to the upper chamber of a transwell coculture system, whereas rat osteoblasts were cultured in the lower chamber. Hence, there was no direct contact between the osteoblasts and WJD/WJF. After coculturing with DMEM supplemented with 10% FBS for 7 days, the expression level of rat *RUNX2* of osteoblasts in ROB/WJD and ROB/WJF groups was higher than that of the ROB group (A and B). Following coculturing for 14 days, the ALP level in osteoblasts were significantly elevated in the ROB/WJD and ROB/WJF groups compared to the ROB group (C and D). At 21 days of coculturing, calcium precipitation level in osteoblasts was significantly increased in the ROB/WJD and ROB/WJF groups compared to the ROB group (E and F). Rat osteoblasts were treated with low molecular weight hyaluronic acid (LHA) or high molecular weight hyaluronic acid (HHA). The expression of osteogenic-related genes was detected *via* RT-qPCR. *RUNX2* increased in all treatment groups (G), while *ALP* and *OPN* did not rise in the ROB + LHA or ROB + HHA groups (H and I). Moreover, the treatment of type 1 collagen (COL1) stimulated the expressions of *RUNX2, ALP, and OPN* in the osteoblasts (J–L). Arrows indicated the cell processes of osteocyte. *, *vs.* the ROB group, $p < 0.05$. #, *vs.* ROB + LHA or ROB + HHA or ROB + COL1 groups, $p < 0.05$.

with alizarin red S to label calcium precipitation. From low to high magnification, mild calcium precipitation was seen in osteoblasts of the ROB alone group. In both the ROB/WJD and the ROB/WJF groups: (1) plenty of calcium precipitation was found surrounding osteoblasts; (2) clusters of osteoblast were observed; (3) cell processes were formed (Fig. 3E). By dissolving calcium precipitation (labeled in dark red, Sigma A5533 and Sigma C-0732) and quantified using absorbance at 540 nm, we found that the level of calcium precipitation was significantly higher in the ROB/WJD and ROB/WJF groups compared with that in the ROB group (Fig. 3F). These results suggested that the components of WJD/WJF dissolving in the medium could promote osteoblasts to differentiate into osteocyte and increase calcium precipitation under the non-contact condition of WJD/WJF and osteoblasts. To investigate which component of WJD/WJF may stimulate osteoblast differentiation and maturation, low molecular weight hyaluronic acid (LHA) and high molecular weight hyaluronic acid (HHA) were added to the culture DMEM with 10%FBS. We observed that the expression level of *RUNX2* of osteoblasts in the groups of ROB/WJD, ROB/WJF, ROB + LHA, and ROB + HHA was significantly higher than that in the ROB alone group (Fig. 3G). The expression of *ALP* and *OPN* of osteoblasts increased in the ROB/WJD and ROB/WJF groups compared to that of the ROB group alone. However, the expression of *ALP* and *OPN* in osteoblasts in the ROB + LHA and ROB + HHA groups was comparable to that in the ROB alone group (Fig. 3H and I). Furthermore, type I collagen, another component of WJD/WJF, was added to the culture DMEM for 7 days to evaluate the effect on the development of osteoblast. The results showed that the expressions of *RUNX2*, *ALP*, and *OPN* of osteoblasts in the groups of ROB/WJD, ROB/WJF, and ROB + COL1 were significantly higher than those in the ROB alone group. The levels of *RUNX2* and *OPN* of osteoblasts increased in the ROB/WJD and ROB/WJF groups compared to those of the ROB + COL1 group (Fig. 3J–L).

The stroma of Wharton's jelly contained high levels of collagens, HA, and several sulfated glycosaminoglycans.[8,10,11] In this study, WJD/WJF had high levels of HA, as well as type I, type III collagen, fibronectin, and muscins (Fig. 1A). *RUNX2* is an early indicator of the osteoblast differentiation and maturation, whereas *OPN* is a late one.[41] *RUNX2* levels increased in all groups (ROB/WJD, ROB/WJF, ROB + LHA, and ROB + HHA), however, LHA and HHA could not trigger an elevation of *OPN*. We suggest that HA may accelerate the early stages of bone formation. WJD/WJF may contain other components like collagen and glycosaminoglycans that contribute to bone formation at different stages. Our results from the co-culture system of osteoblasts and WJD/WJF with non-contact demonstrate that WJD/WJF can function not only as a scaffold but also as a biomaterial for bone repair.

3.4. CT scan showed that both WJD and WJF could individually stimulate osteogenesis in rats with critical-sized calvarial defect

The overall appearances of the skull of the rats were obtained. WJD or WJF were placed in the calvarial defect region (Fig. 4A). We used micro-CT scan to inspect the changes in bone healing in the calvarial bone defect. In the Injury + Saline group, newly formed bone grew only along the boundary of bone defect. In the Injury + WJD and Injury + WJF groups, a newly formed bone was observed not only along the border of the bone defect but also scattered within the defect region (Fig. 4B). The area of newly formed bone within the bone defect region was quantified and presented in percentage. The results showed that the new bone of the Injury + Saline group reached 12.1 ± 1.6% at month 1; however, the speed of new bone formation was extremely slow as time passed, with 17.5 ± 1.1% of new bone at 5 months post-surgery. For the Injury + WJD and Injury + WJF groups, the new bone occupied an area of 21.9 ± 1.9% and 23.0 ± 1.8%, respectively, at one month which were significantly higher than that of the Injury + Saline group ($p < 0.05$). This phenomenon of the marked elevation sustained until month 5 following surgery, with the percentage reaching 29.2 ± 2.0% in the Injury + WJD group and 35.8 ± 1.7% in the Injury + WJF group (Fig. 4C). At month 4, a newly formed bone was substantially higher in the Injury + WJF than that in the Injury + WJD group. Our results revealed that both WJD and WJF could individually promote new bone formation in rats with calvarial defect.

WJF obtained from fresh Wharton's jelly and was immediately frozen in the presence of cryoprotective agents. WJF was readily used after thawing, when it still contained HUMSCs. Xenogeneic transplantation of HUMSCs can repair pulmonary fibrosis, stroke and spinocerebellar ataxia, as well as osteoporosis in rats.[27–32] Transplanted HUMSCs did not only differentiate into osteoblasts, but also stimulate the osteoblasts activity of the recipient in the bone marrow cavity.[30] As a result, WJD/WJF were implanted into rat's skull defects, respectively. After the fourth month of transplantation, the bone formation in the Injury + WJF group increased compared with that in the Injury + WJD group. We suggested that it was because of the existence of HUMSCs in WJF. WJD's 3-dimensional and porous structure can promote osteoblast migration, differentiation, and maturation. It is believed that incorporating mesenchymal stem cells from various sources into WJD, such as bone marrow, umbilical cord, peripheral blood, adipose tissue, skeletal muscle, and dental pulp tissue, will enhance bone repair.[30,42–46] Similar conception, supported by previous studies, indicates that WJD may serve as a scaffold for various cell types to enhance skin healing, cartilage repair, and blood vessel reconstruction.[5–9]

3.5. H&E staining showed that WJD/WJF helped new bone formation in rats with critical-sized calvarial defect

Calvarial tissue sections from each study groups were subjected to H&E staining. The whole injury site in the horizontal sections at low magnification (Fig. 5A), the border of bone defect (Fig. 5B), and the central area of bone defect at high magnification (Fig. 5C) could be observed. In the Injury + Saline group, only a very low amount of newly formed bone was seen around the border (Fig. 5B) but not in the central region of the bone defect, where only deeply stained, connec-

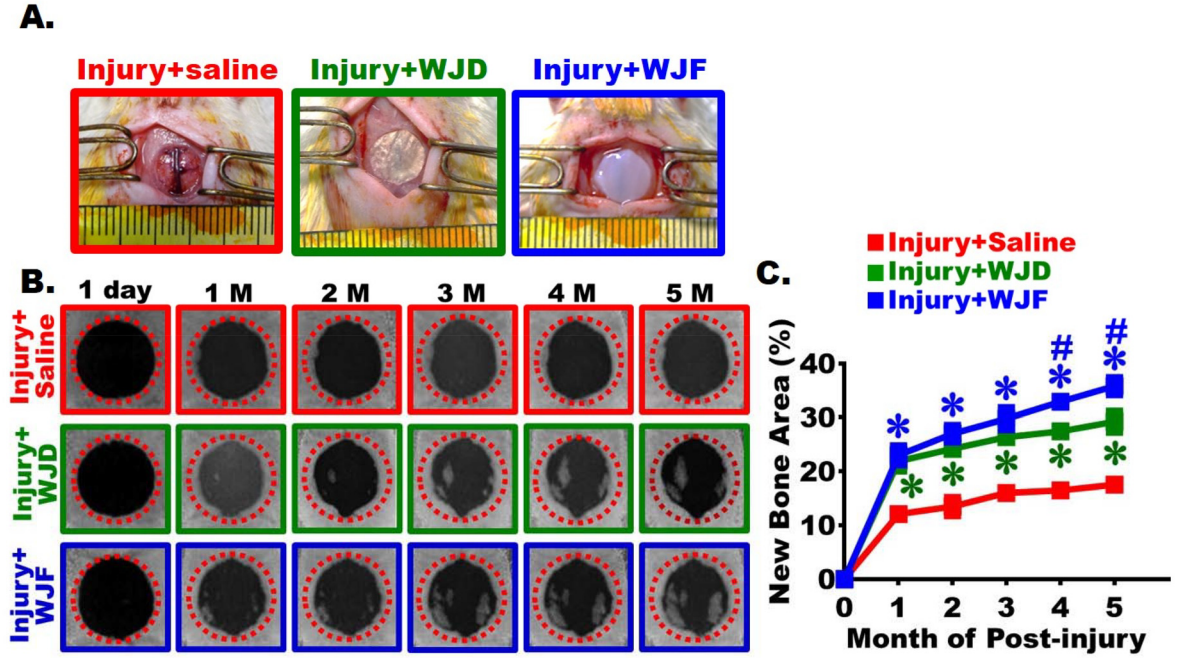

Fig. 4 Micro-CT assessment confirmed that WJD/WJF increased new bone formation in rats with critical-sized calvarial defects. The overall appearances of the skull of the rats were obtained. WJD or WJF were placed in the calvarial defect region (A). At months 1, 2, 3, 4, and 5 following the surgery of critical-sized calvarial defect, the rats were followed up for calvarial healing status *via* micro-CT. In the Injury + Saline group, only a low amount of bone formation along the edge of the bone defect was observed. In the Injury + WJD and Injury + WJF groups, aside from the edge of the bone defect, separate regions with new bone formation were also seen in the central area of bone defect (B). A red dashed line marked the boundary of the bone defect. The percentage of the new bone was significantly higher in the Injury + WJD and Injury + WJF groups compared to the Injury + Saline group (C). *, *vs.* the Injury + Saline group, $p < 0.05$. #, the Injury + WJF group *vs.* the Injury + WJD group, $p < 0.05$.

tive tissue-like structure was observed (Fig. 5C). For the calvaria in the Injury + WJD and Injury + WJF groups, new bone growth was seen not only at the border of defect (Fig. 5B) but also in the central region (Fig. 5C). Bone with a lacunae structure could be observed in the border of the bone defect and the central area of bone defect in the Injury + WJD and Injury + WJF groups.

The area of newly formed bone within the bone defect region was quantified in percentage based on the results of H&E staining. In the Injury + Saline group, the percentage of new bone in the bone defect region was 18.8 ± 1.9%. In the Injury + WJD and Injury + WJF groups, the new bone area was 27.1 ± 4.0% and 32.7 ± 5.0%, respectively, which were significantly higher than that of the Injury + Saline group (Fig. 5D). Microscopy of H&E staining revealed that WJD and WJF could both individually promote new bone formation in rats with calvarial defect.

3.6. Goldner's trichrome staining revealed that WJD/WJF could increase collagen accumulation in rats with critical-sized calvarial defect

Trichrome staining labeled collagen in green and marked its distribution. Both bone-containing lacunae and compact connective tissues appeared in green. The whole injury site in the horizontal sections at low magnification (Fig. 5E), the border of the bone defect (Fig. 5F), and the central area of the bone defect at high magnification (Fig. 5G) could be observed. The results, showing green collagen surrounding the edges of bone defects (Fig. 5E and F) in the Injury + Saline group, indicated that a small amount of new bone had grown at the circumjacent region of the bone defect. In addition, a substantial amount of connective tissue appeared in the central region of the calvarial defect; in some of the regions, collagens stained in green showed a connective tissue-like structure (Fig. 5G). In the Injury + WJD and Injury + WJF groups, new bone was formed along the border of the calvarial defect; hence, green collagen surrounding the defect border was seen (Fig. 5E and F). In addition to the connective tissues that could be clearly observed, a large amount of green collagen also existed at the center of bone defect. At high magnification, bone structure with osteocyte lacunae could be seen clearly (Fig. 5F and G).

At month 5 post-surgery, the area of green collagen within the bone defect region was quantified in percentage based on the results of trichrome staining. In the Injury + Saline group, the percentage of green collagen in the bone defect region was 22.8 ± 1.6%. In the Injury + WJD and Injury + WJF groups, the area with collagen distribution were 42.4 ± 9.7% and 42.9 ± 5.0%, respectively, which were significantly higher, in comparison with that of the Injury + Saline group (Fig. 5H). Hence, trichrome staining, revealed that both WJD or WJF could individually promote collagen formation and accumulation in rats with the calvarial defect.

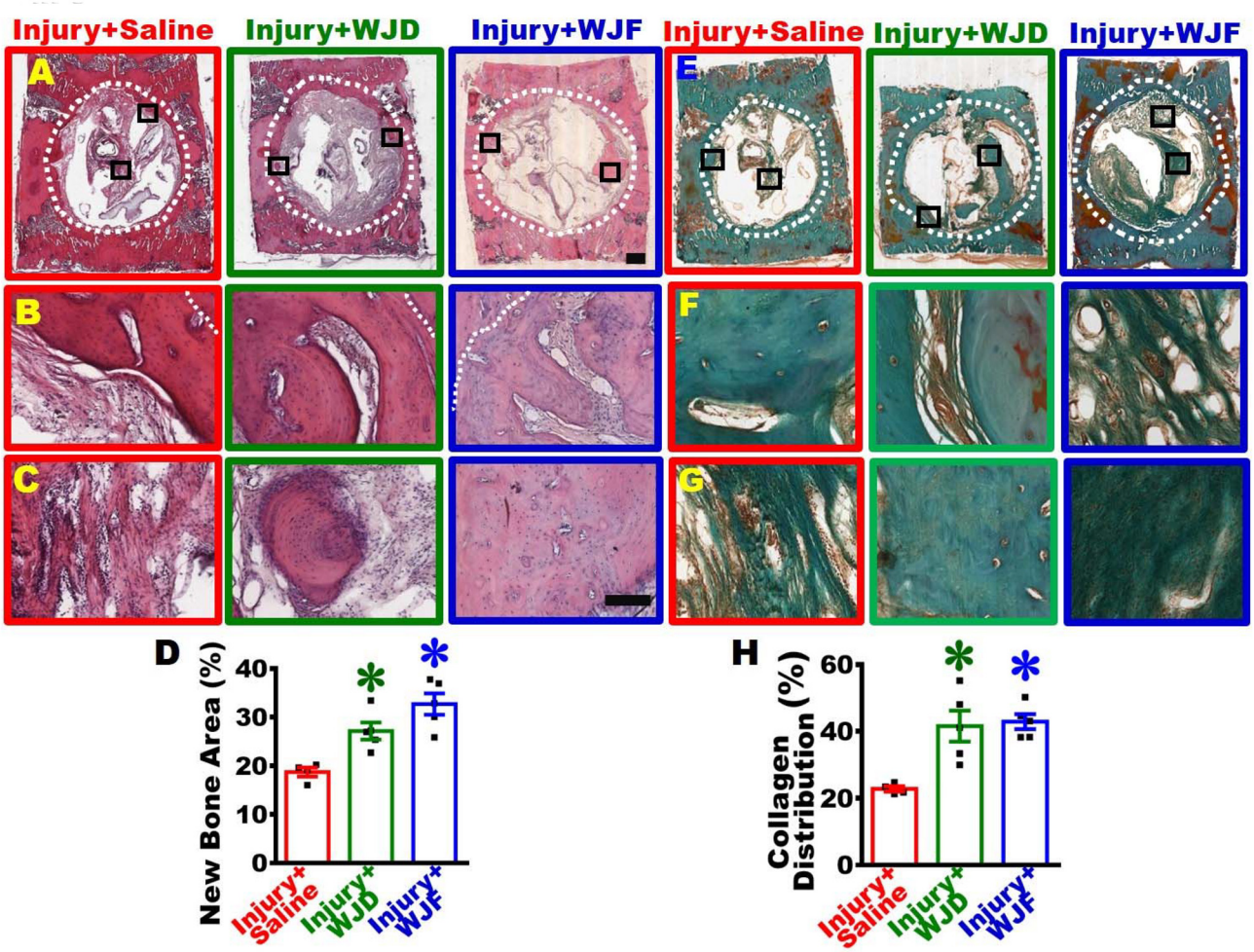

Fig. 5 WJD/WJF improved the bone regeneration in rats with a critical-sized calvarial defect. (A) Horizontal tissue sections from each study group were stained with H&E and photographed at low magnification. The region of the original bone defect is marked with a white dashed line. The border (B) and central regions (C) of bone defect images at high magnification. (D) The percentage of the new bone area was significantly higher in the Injury + WJD and Injury + WJF groups compared to the Injury + Saline group. (E) Horizontal tissue sections from each study group were stained with Goldner's trichrome and photographed at low magnification. The region of the original bone defect is marked with a white dashed line. The border (F) or central regions (G) of the bone defect were shown at a high magnification. (H) The percentage of area covered by collagen in the defect region was quantified based on Goldner's trichrome-stained sections. The results showed that the percentage of area occupied by collagen was significantly higher in the Injury + WJD and Injury + WJF groups compared to the Injury + Saline group. The scale bar represents 1 mm in (A) and (E) and 200 μm in (B), (C), (F), and (G). *, *vs.* the Injury + Saline group, $p < 0.05$.

3.7. Labeling of osteoblasts with alkaline phosphatase staining revealed that WJD/WJF could promote osteoblast maturation in rats with critical-sized calvarial defect

With an ALP staining kit, osteoblast expressing ALP was stained into purple. The whole injury site in the horizontal sections at low magnification (Fig. 6A), the border of bone defect (Fig. 6B), and the central area of the bone defect at high magnification (Fig. 6C) could be observed. In the Injury + Saline group, a layer of cells in purple, representing the location where osteoblasts resided, can be seen (Fig. 6B). At the center of the bone defect, ALP-positive cells were also observed inside the connective tissues (Fig. 6C). For the calvaria in the Injury + WJD and Injury + WJF groups, osteoblasts expressing ALP in several areas were found surrounding the border (Fig. 6B) and at the center region of bone defect (Fig. 6C). Based on the results of ALP staining, the purple-blue region within the bone defect was quantified in percentage. In the Injury + Saline group, the percentage of ALP-positive region was only 3.7 ± 2.1%. In the Injury + WJD and Injury + WJF groups, the ALP-positive region reached 10.0 ± 5.9% and 8.8 ± 2.3%, respectively, which were significantly higher than that of the Injury + Saline group (Fig. 6D). ALP staining, examined *via* optical microscopy, revealed that both WJD and WJF could individually increase the osteoblast level in rats with a calvarial defect.

3.8. WJD/WJF could elevate the osteocalcin level in rat calvarial defect

Osteocalcin, the most abundant non-collagenous bone matrix protein preferentially expressed and secreted by osteoblasts in the late stage of differentiation, could bind to calcium ions to regulate

bone mineralization.[47–49] Immunostaining with anti-osteocalcin was used to label the osteoblasts and uncalcified bone matrix (immature bone area). In immunostaining with anti-osteocalcin, the whole injury site in the horizontal sections at low magnification (Fig. 6E), the border of the bone defect (Fig. 6F), and the central area of the bone defect at high magnification (Fig. 6G) could be observed. In the Injury + Saline group, only a very low and scarce expression of osteocalcin was seen at the border of the bone defect (Fig. 6F); a small amount of osteocalcin was released to connective tissues at the center region of the bone defect (Fig. 6G). In the Injury + WJD and Injury + WJF groups, osteocalcin existed not only at the border but also in the central region of the bone defect. In addition, osteocalcin was also observed in the clusters of osteoblasts, indicating that the osteocalcin was synthesized and secreted by the osteoblasts (Fig. 6F and G).

Based on the results of anti-osteocalcin immunochemical staining, the area of osteocalcin within the bone defect was quantified in percentage. In the Injury + Saline group, the osteocalcin-positive area was 2.4 ± 1.6% of the bone defect. In the Injury + WJD and Injury + WJF groups, the area of osteocalcin significantly increased to 14.8 ± 4.8% and 15.5 ± 1.5%, respectively (Fig. 6H). We speculated that the activity of osteoblasts in the Injury + Saline group was extremely low at month 5 post-surgery, whereas the activity of osteoblasts in the Injury + WJD and Injury + WJF groups were comparatively higher and continued to synthesize and release osteocalcin. Anti-osteocalcin histoimmunochemical staining, examined *via* optical microscopy, revealed that both WJD and WJF could individually trigger osteoblasts to synthesize osteocalcin and promote the formation of organic bone matrix.

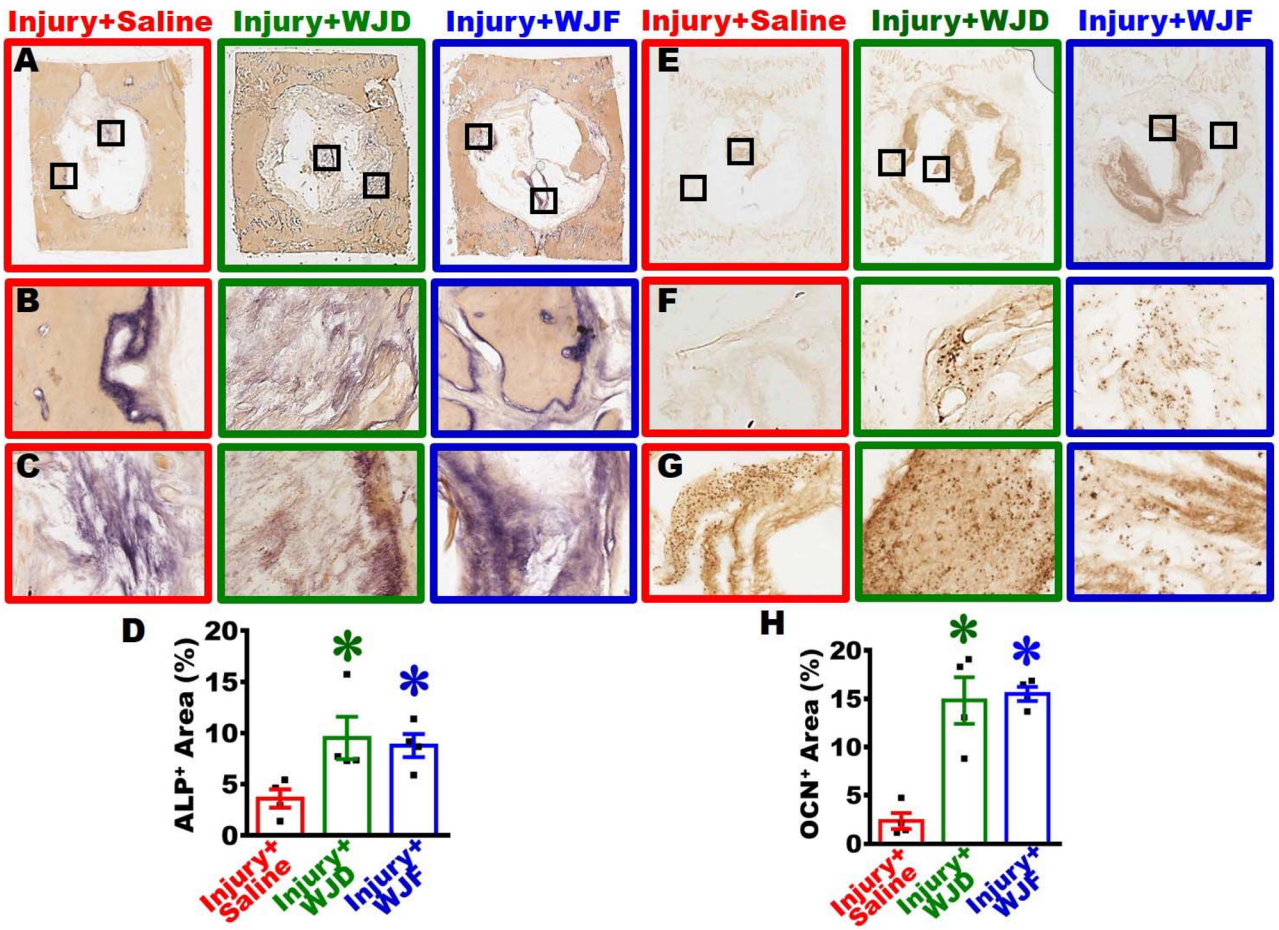

Fig. 6 WJD/WJF promoted the maturation of osteoblasts in critical-sized bone defects. Horizontal tissue sections from each study group were subjected to ALP staining to label osteoblasts in purple (A–C). Micrographs with lower magnification (A) and higher magnification (B and C) show that osteoblasts existed around the border (B) or central regions (C) of bone defect. The percentage of area occupied by osteoblasts in the defect region was quantified based on ALP-stained sections. The results showed that the percentage of area with osteoblast distribution was significantly higher in the Injury + WJD and Injury + WJF groups compared to the Injury + Saline group (D). Horizontal tissue sections from each study group were subjected to immunochemical staining using anti-osteocalcin antibody to label osteocalcin released by osteoblasts. The region of the uncalcified bone matrix is shown in brown. Micrographs with lower magnification (E) and higher magnification (F and G) show the areas containing osteocalcin around the border (F) or central regions (G) of bone defect The percentage of area with osteocalcin in the defect region was quantified based on immunochemically stained sections using anti-osteocalcin antibody. The results showed that the percentage of area with osteocalcin distribution was significantly higher in the Injury + WJD and Injury + WJF groups than in the Injury + Saline group (H). *, *vs.* the Injury + Saline group, $p < 0.05$.

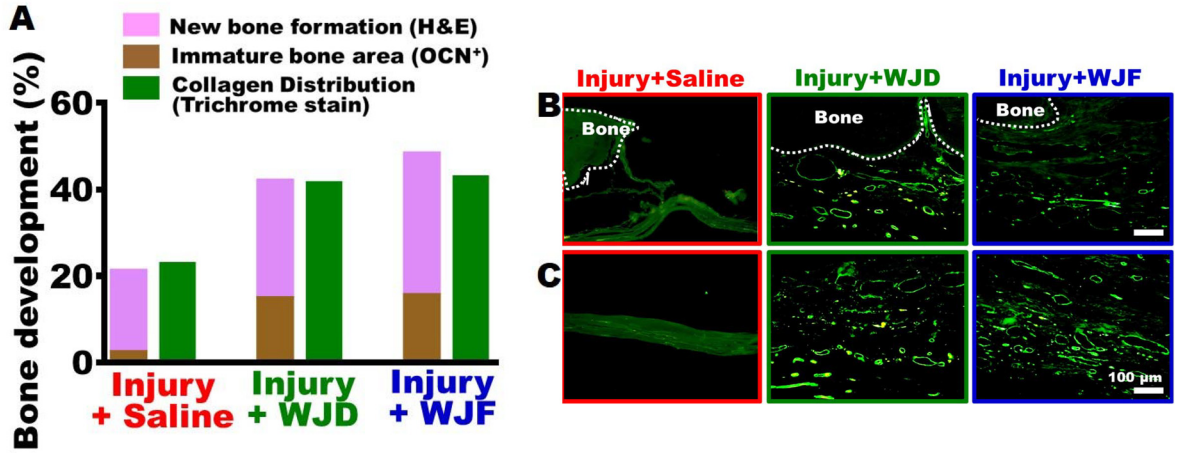

Fig. 7 WJD/WJF markedly promoted the maturation of bone matrix and angiogenesis. The region of uncalcified bone matrix contained or released by osteoblasts was labeled with immunochemical staining using anti-osteocalcin antibodies, and the region of the mature bone matrix was stained with H&E. The quantification data were summed up to evaluate the trend of bone matrix development. The results showed that the trend of bone development in Injury + WJD and Injury + WJF groups was significantly enhanced compared to that of the Injury + Saline group. With Goldner's trichrome staining, collagen within mature bone matrix and/or connective tissues were labeled and quantified. The results showed that study group receiving WJD/WJF had a higher percentage of collagen accumulation. Moreover, the percentage of collagen-accumulating area was comparable to the sum of the percentage of the immature bone area (osteocalcin-positive area) and that of the new bone formation area (H&E staining) (A). (B and C) Blood vessels were labeled with GSL1-B4 (green). High-magnification micrographs of the border (B) and the central regions (C) of bone defect show an extremely small amount of blood vessels at the border and in the central area of bone defect in the Injury + Saline group; in the Injury + WJD and Injury + WJF groups, the number of blood vessels markedly increased.

3.9. Both WJD and WJF could individually promote bone development and maturation substantially

The sum of the percent area of the uncalcified bone matrix contained in or released by osteoblasts quantified *via* anti-osteocalcin (OCN) immunostaining and mature bone matrix quantified *via* H&E staining represented the trend of bone development and maturation. Our results showed that the level of bone development was approximately 21% in the Injury + Saline group. For the Injury + WJD and Injury + WJF groups, the level of bone development was around 42% and 48%, respectively, and was significantly higher than that of the Injury + Saline group. The percentages of bone development and maturation were comparable to the results of trichrome staining (Fig. 7A). The horizontal calvarial sections were stained with trichrome staining to label the collagen green. Trichrome staining revealed collagen distribution, which could be detected not only in mature bone with bone lacuna, but also in connective tissues, where there may be immature bone matrix deficient in calcium. The administration of WJD/WJF improves bone healing by approximately 50%, indicating that the lesion was not completely repaired. In future studies, we will explore the efficacy of the combination WJD/WJF with other growth factors, such as bone morphogenetic protein-2 for the potential clinical application of bone defect.[50]

3.10. Both WJD and WJF could individually increase angiogenesis in rats with critical-sized calvarial defect

Vascular endothelial cells were labeled with GSL1-B4 to observe the distribution of blood vessels. In the Injury + Saline group only a few blood vessels were seen either at the border or in the central region of bone defect. In contrast, in the Injury + WJD and Injury + WJF groups, a substantial amount of blood vessels were found not only at the border but also in the central region of the bone defect (Fig. 7B and C). Numerous studies have demonstrated that vascularization plays a critical role in skeletal regeneration. The fast-established circulatory system transports essential materials such as nutrition, oxygen, and growth factors in order to stimulate osteogenesis.[51,52]

Previous research studies have shown that transplantation of umbilical cord mesenchymal stem cells can increase angiogenesis.[31,53] This study reveals that the composition of WJD/WJF could stimulate the growth of bone and blood vessels. WJD/WJF can be used alone in bone-damaged or bone-lost areas. Additionally, WJD/WJF can also be integrated with other medical materials such as synthetic hydrogel, autologous or allogeneic bone treated with liquid nitrogen or chemicals, to accelerate bone formation, and thereby ensuring bone rigidity to reduce the risk of fractures before bone recovery. Although there is a limited supply of human umbilical cords, WJD is free of umbilical cord mesenchymal stem cells, and umbilical cords from various animals, such as cattle, deer, and pigs, can also be used as sources for clinical medicine.

4. Conclusions

WJF/WJD could act as great scaffolds to promote new bone formation for application in clinical medicine. Furthermore, their components could facilitate bone regeneration and serve as

natural therapeutic medical materials for patients suffering from bone defect and bone loss. Regarding the safety, efficacy and convenience for clinical trials, among the two products of Wharton's jelly, WJD was processed and lyophilized in the absence of cryoprotective agents to form a three-dimensional porous structure free of HUMSCs. Taking into account that WJD is convenient for preservation and transportation, it is an ideal medical bone material.

Institutional review board statement

All animal procedures were performed in accordance with the Guidelines for Care and Use of Laboratory Animals of National Yang Ming Chiao Tung University and approved by the Animal Ethics Committee of National Yang Ming Chiao Tung University (IACUC Approval no 1100313). The use of human umbilical cords in this study was approved by the Research Ethics Committee of Taipei Veterans General Hospital (IRB Approval 202101008BC).

Author contributions

Fu YS and Chen CF designed the experiments; acquired, analyzed and interpreted the data; and drafted the manuscript. Yeh CC and Chen TH supported the materials; Tong ZJ and Tsai SW acquired, analyzed, and interpreted the data; and contributed to the manuscript. All authors approved the final version.

Data availability

All the data supporting the findings will be made public and can be shared by contacting the corresponding author CF Chen and the first author YS Fu.

Conflicts of interest

The authors declare that they have no known competing financial interests or personal relationships that could have appeared to influence the work reported in this paper.

Acknowledgements

This work was supported by the MOST 109-2314-B-075-093 grant from the Ministry of Science and Technology, V111C-012 and V113C-180 grants from Taipei Veterans General Hospital, and grants 111-018, 112-027, 113-001 from the Lung Cancer Foundation in Memory of Kwang-Shun Lu. We wish to thank Dr Arthur Er-Terg Chiou of the Institute of Biophotonics at the National Yang Ming Chiao Tung University for his invaluable help in reviewing the manuscript and helpful suggestions for language editing.

References

1 E. Roddy, M. R. DeBaun, A. Daoud-Gray, Y. P. Yang and M. J. Gardner, *Eur. J. Orthop. Surg. Traumatol.*, 2018, **28**(3), 351–362.
2 J. P. Vacanti and R. Langer, *Lancet*, 1999, **354**, 32–34.
3 E. M. Ahmed, *J. Adv. Res.*, 2015, **6**, 105–121.
4 T. C. Ho, C. C. Chang, H. P. Chan, T. W. Chung, C. W. Shu, K. P. Chuang, T. H. Duh, M. H. Yang and Y. C. Tyan, *Molecules*, 2022, **27**(9), 2902.
5 D. Li, G. Chiu, B. Lipe, R. A. Hopkins, J. Lillis, J. M. Ashton, S. Paul and O. S. Aljitawi, *Blood Adv.*, 2019, **3**(7), 1011–1026.
6 L. Lin, Y. Xu, Y. Li, X. Gong, M. Wei, W. Zhang, X. Zhang and Y. Xu, *Mater. Des.*, 2020, **186**, 108216.
7 P. Gupta, G. R. Chaudhuri, G. Janani, M. Agarwala, D. Ghosh, S. K. Nandi and B. B. Mandal, *Adv. Healthcare Mater.*, 2021, **10**(19), 2100750.
8 B. Beiki, B. Zeynali and E. Seyedjafari, *Mater. Sci. Eng., C*, 2017, **78**, 627–638.
9 M. Cooke, E. Tan, C. Mandrycky, H. He, J. O'Connell and S. Tseng, *J. Wound Care*, 2014, **23**(10), 465–476.
10 S. Franc, J. C. Rousseau, R. Garrone, M. van der Rest and M. Moradi-Ameli, *Placenta*, 1998, **19**(1), 95–104.
11 I. Arutyunyan, A. Elchaninov, A. Makarov and T. Fatkhudinov, *Stem Cells Int.*, 2016, **2016**, 6901286.
12 V. R. Sherman, W. Yang and M. A. Meyers, *J. Mech. Behav. Biomed. Mater.*, 2015, **52**, 22–50.
13 A. M. Ferreira, P. Gentile, V. Chiono and G. Ciardelli, *Acta Biomater.*, 2012, **8**(9), 3191–3200.
14 D. Qin, N. Wang, X.-G. You, A.-D. Zhang, X.-G. Chen and Y. Liu, *Biomater. Sci.*, 2022, **10**(2), 318–353.
15 M. Hemshekhar, R. M. Thushara, S. Chandranayaka, L. S. Sherman, K. Kemparaju and K. S. Girish, *Int. J. Biol. Macromol.*, 2016, **86**, 917–928.
16 P. Zhai, X. Peng, B. Li, Y. Liu, H. Sun and X. Li, *Int. J. Biol. Macromol.*, 2020, **151**, 1224–1239.
17 T. Khaliq, M. Sohail, M. U. Minhas, A. Mahmood, A. Munir, A. H. M. Qalawlus, N. Jabeen, M. Kousar and Z. Anwar, *Int. J. Pharm.*, 2023, **643**, 123244.
18 B. Li, P. Gao, H. Zhang, Z. Guo, Y. Zheng and Y. Han, *Biomater. Sci.*, 2018, **6**(12), 3202–3218.
19 S. Hemmati-Sadeghi, J. Ringe, T. Dehne, R. Haag and M. Sittinger, *Int. J. Mol. Sci.*, 2018, **19**(5), 1519.
20 S. E. Kim, J. Y. Lee, K.-S. Shim, S. Lee, K. Min, J.-H. Bae, H.-J. Kim, K. Park and H.-R. Song, *Int. J. Biol. Macromol.*, 2018, **114**, 341–348.
21 G. Agarwal, S. Agiwal and A. Srivastava, *Int. J. Biol. Macromol.*, 2020, **165**, 388–401.
22 H. Y. Jang, J. Y. Shin, S. H. Oh, J.-H. Byun and J. H. Lee, *ACS Biomater. Sci. Eng.*, 2020, **6**(9), 5172–5180.
23 L. Wang, X. Nan, J. Hou, Y. Xia, Y. Guo, K. Meng, C. Xu, J. Lian, Y. Zhang and X. Wang, *Biomed. Mater.*, 2021, **16**(4), 045045.
24 L. Liu, W. Jia, Y. Zhou, H. Zhou, M. Liu, M. Li, X. Zhang, G. Gu and Z. Chen, *Int. J. Biol. Macromol.*, 2022, **206**, 277–287.

25 N. M. Ocarino, J. N. Boeloni, A. M. Goes, J. F. Silva, U. Marubayashi and R. Serakides, *Nitric Oxide*, 2008, **19**(4), 320–325.
26 X. Qiao, Y. Nie, Y. Ma, Y. Chen, R. Cheng, W. Yin, Y. Hu, W. Xu and L. Xu, *Sci. Rep.*, 2016, **6**, 18732.
27 K. A. Chu, S. Y. Wang, C. C. Yeh, T. W. Fu, Y. Y. Fu, T. L. Ko, M. M. Chiu, T. H. Chen, P. J. Tsai and Y. S. Fu, *Theranostics*, 2019, **9**(22), 6646.
28 K. A. Chu, C. C. Yeh, F. H. Kuo, W. R. Lin, C. W. Hsu, T. H. Chen and Y. S. Fu, *Stem Cell Res. Ther.*, 2020, **11**(1), 513.
29 K. A. Chu, C. C. Yeh, C. H. Hsu, C. W. Hsu, F. H. Kuo, P. J. Tsai and Y. S. Fu, *Int. J. Mol. Sci.*, 2023, **24**(8), 6948.
30 Y. S. Fu, C. H. Lu, K. A. Chu, C. C. Yeh, T. L. Chiang, T. L. Ko, M. M. Chiu and C. F. Chen, *Cell Transplant.*, 2018, **27**(1), 194–208.
31 Y. S. Fu, C. C. Yeh, P. M. Chu, W. H. Chang, M. Y. A. Lin and Y. Y. Lin, *Int. J. Mol. Sci.*, 2022, **23**(6), 3149.
32 P. J. Tsai, C. C. Yeh, W. J. Huang, M. Y. Min, T. H. Huang, T. L. Ko, P. Y. Huang, T. H. Chen, S. P. Hsu and B. W. Soong, *Transl. Neurodegener.*, 2019, **8**, 29.
33 F. M. Hansen-Smith, L. Watson, D. Y. Lu and I. Goldstein, *Microvasc. Res.*, 1988, **36**(3), 199–215.
34 F. Copes, N. Pien, S. Van Vlierberghe, F. Boccafoschi and D. Mantovani, *Front. Bioeng. Biotechnol.*, 2019, **7**, 166.
35 C. Dong and Y. Lv, *Polymers*, 2016, **8**(2), 42.
36 C. Valentino, B. Vigani, G. Zucca, M. Ruggeri, C. Boselli, A. I. Cornaglia, L. Malavasi, G. Sandri and S. Rossi, *Int. J. Biol. Macromol.*, 2023, **242**, 125000.
37 L. Teixeira, G. Crippa, L.-P. Lefebvre, P. De Oliveira, A. L. Rosa and M. M. Beloti, *Int. J. Oral Maxillofac. Surg.*, 2012, **41**(9), 1097–1101.
38 F. L. He, D. W. Li, J. He, Y. Y. Liu, F. Ahmad, Y. L. Liu, X. Deng, Y. J. Ye and D. C. Yin, *Mater. Sci. Eng., C*, 2018, **86**, 18–27.
39 C. M. Murphy, G. P. Duffy, A. Schindeler and F. J. O'brien, *J. Biomed. Mater. Res., Part A*, 2016, **104**(1), 291–304.
40 D. G. Bello, A. Fouillen, A. Badia and A. Nanci, *Acta Biomater.*, 2017, **60**, 339–349.
41 Z. Tang, X. Li, Y. Tan, H. Fan and X. Zhang, *Regener. Biomater.*, 2018, **5**(1), 43–59.
42 Y. Liu, R. Yang and S. Shi, *Tissue Eng., Part A*, 2015, **21**(3–4), 498–509.
43 C. Wan, Q. He and G. Li, *J. Orthop. Res.*, 2006, **24**(4), 610–618.
44 S. M. Wilson, M. S. Goldwasser, S. G. Clark, E. Monaco, M. Bionaz, W. L. Hurley, S. Rodriguez-Zas, L. Feng, Z. Dymon and M. B. Wheeler, *J. Oral Maxillofac. Surg.*, 2012, **70**(3), e193–e203.
45 A. Julien, A. Kanagalingam, E. Martínez-Sarrà, J. Megret, M. Luka, M. Ménager, F. Relaix and C. Colnot, *Nat. Commun.*, 2021, **12**(1), 2860.
46 C. Vater, C. Männel, J. Bolte, X. Tian, S. B. Goodman and S. Zwingenberger, *Curr. Stem Cell Res. Ther.*, 2022, **17**(5), 480–491.
47 G. Wolf, *Nutr. Rev.*, 1996, **54**(10), 332–333.
48 M. F. Young, *Osteoporosis Int.*, 2003, **14**, 35–42.
49 J. P. Gorski, *Front. Biosci.*, 2011, **16**, 2598–2621.
50 C. E. Vantucci, L. Krishan, A. Cheng, A. Prather, K. Roy and R. E. Guldberg, *Biomater. Sci.*, 2021, **9**(5), 1668–1682.
51 J. Ma, S. Wu, J. Liu, C. Liu, S. Ni, T. Dai, X. Wu, Z. Zhang, J. Qu, H. Zhao, D. Zhou and X. Zhao, *Biomater. Sci.*, 2022, **10**(16), 4635–4655.
52 C. Wang, W. Lu and M. Wang, *J. Mater. Chem. B*, 2020, **8**, 636–647.
53 Y. C. Lin, T. L. Ko, Y. H. Shih, M. Y. Lin, T. W. Fu, H. S. Hsiao, J. Y. Hsu and Y. S. Fu, *Stroke*, 2011, **42**(7), 2045–2053.